Yeboah, D., Gkantou, M., Investigation of flexural behaviour of structural timber beams strengthened with NSM basalt and glass FRP bars. Structures 33(6):390-405.
https://doi.org/10.1016/j.istruc.2021.04.044

Authors: David Yeboah[1], Michaela Gkantou[1,*]

[1]School of Civil Engineering and Built Environment, Liverpool John Moores University, UK

[*]Corresponding author: Michaela Gkantou, Email: m.gkantou@ljmu.ac.uk

ABSTRACT

Near Surface Mounted (NSM) fibre reinforced polymer (FRP) bars is an effective technique of improving the performance of timber beams. Despite the potential of NSM technique, literature remains limited, whilst there is not any standard method for the prediction of the NSM FRP timber flexural capacity. Extending the pool of experimental data and thus the understanding of FRP strengthened timber structures, the present paper reports an experimental study of timber beams reinforced with glass and basalt FRP bars. Moreover, the paper presents a general theoretical model in order to estimate the moment resistance of the NSM FRP timber beams. The experimental study examined white spruce timber specimens in two reinforcement configurations; one with reinforcement bars only on the tension zone and one with reinforcement bars both on the tension and the compression zone. Control specimens were also included for comparison purposes. All beams had a rectangular cross-section of 70×215 mm and were loaded under four-point bending configuration with a 2.3 m span. A total of 20 specimens were tested under displacement control quasi-static monotonic loading. The main failure mechanism observed for both NSM FRP reinforced and unreinforced specimens was brittle tensile failure of the timber at the tensile zone. The load-deflection curves, the strain distribution profiles and the failure modes were discussed. It was observed that a significant increase on the ultimate load (33% – 69%) and the flexural stiffness (22% – 33%) of the timber beams can be achieved due to the NSM reinforcement. The proposed theoretical model for the ultimate strength of NSM FRP strengthened timber beams is assessed on the basis of the test results and collated data, showing a good comparison between the experimental and theoretical results.

Keywords: timber beams, Near Surface Mounted (NSM), BFRP, GFRP, flexural behaviour

Highlights:

- 20 four-point bending tests on timber beams.
- NSM BFRP and GFRP reinforced timber beams were studied.
- The flexural behaviour was improved by FRP reinforcement.
- A theoretical model able to predict the flexural strength was presented

Nomenclature:

A_{fc} Cross-sectional areas of FRP bars at compression zone

A_{ft} Cross-sectional areas of FRP bars at tensile zone

b Width of the cross-section

E_f Modulus of Elasticity of FRP

EI Flexural rigidity

E_w Modulus of Elasticity of timber

F_{fc} Force of FRP in compression

f_{fcu} Compressive strength of FRP

F_{ft} Force of FRP in tension

f_{ftu} Tensile strength of FRP

F_{wc1} Force of timber in compression (plastic region)

F_{wc2} Force of timber in compression (elastic region)

f_{wcy} Compressive strength of timber

F_{wt} Force of timber in tension

f_{wtu} Tensile strength of timber

h Depth of the cross-section

I Second moment of area

k Stiffness

k_{exp} Experimental stiffness

k_{theor} Theoretical stiffness

L Span of the beam

M_u Failure moment

$M_{u,exp}$ Experimental failure moment

$M_{u,theor}$ Theoretical failure moment

N_u Failure load

x_c Depth of the compression zone

x_{c1} Depth of the compression zone in plastic region

x_{c2} Depth of the compression zone in elastic region

x_t Depth of the tension zone

z_{fc} Distance of the centre of the FRP compression bars from the beam's edge

z_{ft} Distance of the centre of the FRP tensile bars from the beam's edge

α Distance from loading point to support

ΔP Range of the applied load

δ_{theor} Theoretical mid-span vertical displacement at failure assuming linear response

δ_u Mid-span vertical displacement at failure

$\delta_{u,exp}$ Experimental mid-span vertical displacement at failure

$\Delta\delta$ Range of the mid-span vertical displacement

E Modulus of Elasticity

ε_f Strain of FRP

ε_{fcu} Ultimate compressive strain of FRP

ε_{ftu} Ultimate tensile strain of FRP

ε_w Strain of timber

ε_{wcu} Ultimate compressive strain of timber

ε_{wcy} Yield compressive strain of timber

ε_{wtu} Ultimate tensile strain of timber

σ_f Stress of FRP

σ_w Stress of timber

1. INTRODUCTION

Strengthening of timber structures is required due to deterioration resulting from poor maintenance, accidental damage or need for extension of the design life of structures [1]. Reinforcement with steel or fibre reinforced polymer (FRP) materials is an effective method of improving the strength and stiffness of timber structures [2, 3]. The use of FRPs as strengthening materials has advantages compared to steel, such as higher strength-to-weight ratio and better resistance to corrosion [4]. FRP composite materials are used in the construction industry for repair, rehabilitating, retrofitting and strengthening structures [5, 6]. The two main forms of FRP composites used in timber reinforcements are externally and internally and bonded systems. In case of externally bonded reinforcement (EBR), FRP plates or fabrics are employed at the tensile region of a structure [7-9]. Structures strengthened with the EBR method have been found to exhibit bond fracture between the concrete and FRP members, whereas the reinforced bars or plates are exposed to the effect of fire or vehicular movements [10]. For internally bonded systems, pultruded bars and plates are normally glued into grooves or slots of timber members and this type of reinforcement is known as near surface mounted (NSM) reinforcement. Due to larger interfacial bond between the host structural material and the adherents as well as greater anchorage of the bars into adjacent host member, NSM has improved load and bond capacity [11,12] compared to EBR, whilst the host timber protects the FRP from damages [8]. Moreover, in NSM method, the aesthetic nature of the strengthened structure is preserved [11].

NSM technique in strengthening timber structures was introduced recently and therefore its application is mainly based on the literature [13]. Research studies on the use of NSM FRP reinforcement demonstrated increased flexural strength and stiffness of the timber beams [14-17]. Long-term research on the flexural strength has also shown the potential of the NSM technique [18]. Theoretical and finite element methods able to predict the capacities and behaviours of the reinforced beams have been reported [17-20]. In addition, the NSM technique has been used to strengthen 75 stringers of a 10m long span bridge, near Winnipeg in Canada [15]. Poletti et al. [13] assessed the effectiveness of NSM as a retrofitting technique for the improvement of stiffness, ductility, lateral resistance and dissipation of energy of timber frame walls. The NSM method has also been used to rehabilitate traditional floors [21], employing both steel and FRP structures. These reinforcement or rehabilitation methods by the NSM method create sustainability, which is very important on the basis of environmental, economic, historical and social aspects [1].

Even though research shows that the NSM FRP technique leads to significant improvement in the performance of timber structures, literature still remains limited, compared to EBR technique. Currently, there is no established design calculations in European and international structural design

standards regarding the use of the NSM technique. Additional research on the behaviour of this innovative technique is required for full-scale implementation. The current paper presents an experimental investigation of timber beams reinforced with NSM FRP bars. The influence of the bar type and the design configuration are examined. Theoretical predictions are also presented and compared with the test results.

2. BACKGROUND AND PREVIOUS RESEARCH

2.1 FRP reinforcements

FRPs are composite materials manufactured by the combination of at least two materials resulting in a material of different properties. FRPs differ from other composite materials, since both the constituent materials, as well as their structural compositions control their physical and mechanical properties. The composite is made up of fibres and a polymer matrix bonded together by an adhesive. The fibres contain about 30%-70% and 50% of the composite by volume and weight, respectively. The mechanical properties of the composite are determined by the integrity of the fibres, whereas the polymer matrix determines the rigidity and protection against the environmental factors [22,23]. There are different forms of FRPs with corresponding different mechanical as well as physical properties, which depend on the fibres amount and orientation [24,25]. In structural engineering, the most common types of FRPs are glass (GFRP), carbon (CFRP), basalt (BFRP) and aramid (AFRP). The most abundant type of the FRPs is the GFRP. Glass fibres are one of the most well-established composite materials currently used in a wide range of industrial applications with reported usage in bridges and highways [26, 27]. GFRP composite materials are significantly lighter than the composite materials fabricated of timber and steel, as the GFRP strength-to-weight ratio is higher than that of steel. Basalt is a relatively new FRP material, compared to GFRP and CFRP [28]. Basalt fibres are environmentally friendly since they produce non-toxic reaction in contact with water or air and they are also not combustible. BFRP bars are used in the construction and highway industry due to their stiffness and thermal performance [29]. AFRPs have the lowest density and the best strength-to-weight ratio, while are rapidly degraded by ultraviolet light and therefore should be coated or painted [6]. CFRP composites that are employed in structural strengthening and reinforcement [30] are made from polyacrylonitrile filaments, which result in improved material quality. CFRPs are about 10-30 times more expensive than the corresponding GFRP or BFRP types [31].

2.2 Groove filler for NSM technique

The adhesive used in the NSM technique is a groove filler and acts as the medium through which shear stresses are transferred between the host timber and the FRP bars. Hence, the most important structural properties of the groove filler in the current technique are the shear and tensile strength [11]. Several engineering adhesives have been employed in the experimental investigation of NSM FRP samples. Phenol-resorcinol, Sikadur 31 and epoxy resins have been applied in [32,33], whilst the 2-part epoxy is the most common adhesive used for NSM technique [15]. In 2-part epoxy adhesives, one component is the base, containing epoxy resin and the second component is the curing agent or hardener. Epoxy adhesives have high shear strength and are able to resist temperature between -40°C to 100°C, while they are relatively economical and easy to use [34].

2.3 Reinforcement configuration of NSM FRP timber structures

The NSM specimens are fabricated by cutting grooves into the structural timber and the FRP bars or plates are bonded into the prefilled adhesive [16]. Figure 1 shows typical configurations of NSM FRP timber structures. Past research on low-grade glulam timber beams reinforced with GFRP bars showed that circular grooves allowed for higher improvements on the stiffness and moment capacity compared to square grooves [33]. The reinforcement ratios can also influence the performance; strength improvements in the range of 18% and 46% for reinforcement ratios between 0.27% and 0.82%, respectively have been reported [15], whilst for single or low reinforcement ratios, stiffness has not shown significant improvement [35]. For enhanced strength performance, 25% and 75% of the reinforcement was suggested to be at the top and bottom of the timber beam section, respectively, whereas for enhanced stiffness, equal reinforcement at the tensile and compression zone was recommended [35]. For maximum ductility, all of the reinforcement was suggested to be placed on the bottom [35]. Past research has also compared the bending behaviour of CFRP NSM plates and rods with NSM technique [35, 36].

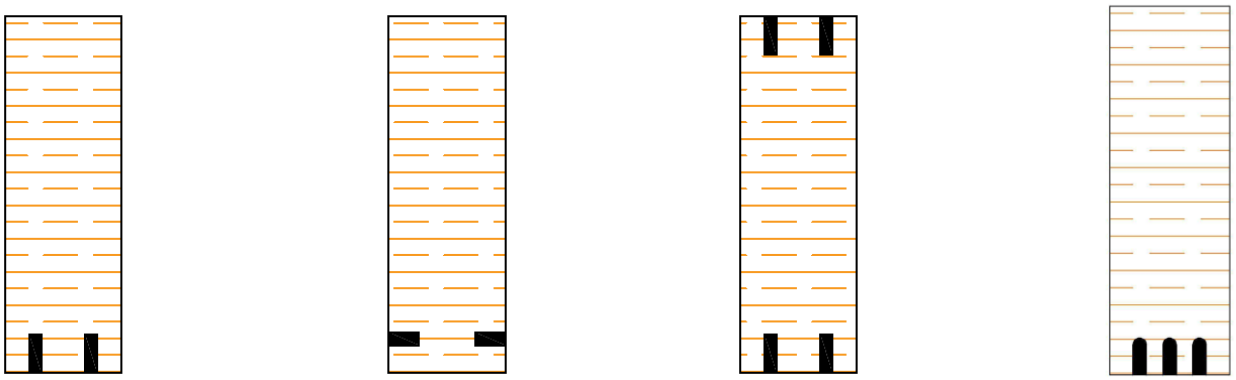

Bottom single reinforced with 2 bars in rectangular grooves

Bottom single reinforced with 2 bars in rectangular grooves on lateral sides

Bottom and top double reinforced with 2 bars in rectangular grooves

Bottom single reinforced with 3 bars in circular grooves

Figure 1: Examples of NSM reinforcement configurations.

2.4 Bond behaviour of NSM technique

Within composite structures, the ultimate capacity and the deformation of the reinforced system is also determined by the behaviour of the bond and thus research has been carried out to examine the bond behaviour of NSM structures [37,38]. At NSM technique, the transfer of stresses is achieved by chemical adhesion. The interaction and transfer of stresses occur at two main interfacial zones. Firstly, stress transfer occurs along the interface between the bar and the adhesive. Secondly, stresses can be transferred along the interface surrounding the adhesive and the host timber. Surface roughness, dimensions of groove, and the adhesive's behaviour determine the bond capacity. When the reinforced structure is subjected to loading, the force is transferred through the NSM bond and the FRP bar contributes to bond resistance. Mechanical interlocking which may occur when the reinforced bar has rough surface [39-41] also contributes to bond strength. De Lorenzis [42] has suggested that, for round bars, the minimum value of a constant, k (where k = ratio of groove width to nominal diameter of the bar) should be 1.5 for smoothly or lightly sand-blasted bars and a value of 2.0 for deformed bars.

2.5 Failure mode of NSM FRP timber beams

Experimental investigations on bending tests of NSM FRP specimens have been carried out and two main failure mechanisms have been reported. Firstly, splitting failure can occur at the tension zone of the beam before the compression zone has yielded [33,36]. Secondly, tensile failure by splitting can occur together with yielding at the compression zone of the beam [36]. The amount of FRP reinforcement was reported to affect the failure mechanism of the timber beams [43]. FRP bars are capable of arresting crack openings, restraining rupture and bridging timber defects [19,20] and for

increasing reinforcement at the tension zone, the failure mode can change from brittle to ductile behaviour [33, 36, 38]. Failure involving FRP fracture and cohesive failure of adhesive have not been reported.

2.6 Past research work on NSM FRP timber beams and research significance

Research work on NSM FRP strengthened timber is summarised in Table 1. Previous experiments used different FRP reinforcement type and configurations. Both single and double reinforcement configurations have been examined, whilst [43] reported that maximum flexural strength could be obtained if 75% of the reinforcement is on the bottom face and 25% on the top of the beam. As can be seen in Table 1, there are many studies on CFRP reinforcements, whereas a lot of focus has been placed on laminated timber. Extending the pool of experimental data, this paper will examine white spruce structural timber and the strength enhancement due to BFRP and GRFP bars in two different configurations. As a novel technique, the selected arrangements aimed to firstly assess the increase in the strength due to two bars on the bottom (100% reinforcement on the tension zone) and then to examine the performance due to two bars on the bottom and one bar on top (66.6% of the reinforcement on the tension zone and 33.3% on the compression). The present experimental study contributes to enhanced understanding of FRP strengthened timber beams. Moreover, in the absence of a standard method for the prediction of the NSM FRP timber flexural capacity, the paper presents a general theoretical model in order to estimate the moment resistance of the NSM FRP timber beams (Section 5).

Table 1: Past research work of FRP NSM strengthened timber beams *(in reverse chronological order)*.

Reference	Timber species	Type of FRP	Configuration	No of tests
Gentile et al (2002) [15]	Douglas fir	GFRP bars	a) 4 bars bottom; b) 4 bars bottom at lateral sides	26
Johnsson et al (2007) [14]	Glulam lamella	CFRP bars	a) 1 bar bottom; b) 2 bars bottom	10
Kliger et al (2008) [43]	Glulam	CFRP plates	a) 5 plates bottom and 5 top; b) 5 plates bottom and 3 top	6
Raftery and Whelan (2014) [33]	Irish grown Sitka spruce	GFRP bars	a) 2 bars bottom; b) 3×2 bars bottom; c) 2 bars bottom and circular grooves; d) 2 bars bottom and square grooves; e) 2 bars bottom and 2 top	25
Raftery and Kelly (2015) [2]	Low-grade glued laminated timber	BFRP bars	a) 4 bars bottom; b) 2 bars bottom at lateral sides	30
Lu et al (2015) [16]	Douglas fir and Poplar	CFRP laminates	a) 2 bars bottom; b) 3 bars bottom; c) 3 bars bottom and 3 bars top	24
Yang et al (2016) [19]	Douglas fir glulam	GFRP bars and plates, CFRP bars	a) 1 bar bottom; b) 2 bars bottom; c) 2 bars bottom-lateral sides and 1 top; d) 1 plate bottom; e) 1 plate bottom and 1 top; f) 2 plates bottom; g) 3 plates bottom; h) 3 plates bottom and 3 top	16
Chun et al (2016) [36]	Small fir and pine Timber	CFRP plates and bars	a) 1 bar bottom; b) 1 plate bottom	20
Xu et al (2017) [18]	Douglas fir	CFRP bars	a) 1 bar bottom	3
Xueyu et al (2018) [20]	Fir wood (Hui-style)	CFRP bars and plates	a) 4 bars bottom; b) 1 plate bottom	5
Bakalarz et al (2020) [44]	laminated veneer lumber	CFRP laminates	a) 1 laminate bottom	10

3. EXPERIMENTAL PROGRAMME

3.1 Materials

The materials used for the experiments of the present study were structural timber, BFRP and GFRP bars and epoxy adhesives. The diameter of the employed reinforcement bars was 8 mm.

Basalt originates from volcanic magma or volcanoes with very high temperature found in the earth crust. It comes with different colours mostly grey, brown or dark [45]. The BFRP bars used herein had grey colour and with coarse-grain sanded finish for improved bonding. The fibres were manufactured with extrusion by melting crushed basalt (rock) at 1400°C [46] and were then formed with application of lubricants, followed by winding [45, 47]. BFRP bars were used for the present research due to their availability and relatively low price. In addition, basalt FRP has improved fire resistance, better resistance to chemically environment compared to glass fibres. Commercial glass fibres, as those used in this study, are manufactured from silica, which are melted to temperature as high as 1400°C. The next stage is the extrusion of the molten glass, which is then cooled. The filaments are then sized, forming strand and wound on a drum. A mixture of lubricants are added to improve the wettability of

the fibres, providing better adhesion between the fibre components [46]. Glass fibres are less brittle compared to other FRPs and the raw materials are relatively inexpensive. The bulk strength and properties of weight of GFRP, are considerably more favourable in comparison to steel. The fibres in GFRP bars resist tensile and compressive loads, whilst the resin transfer shear loads [25]. In this project, GFRP bars were chosen due to their availability, favourable strength and mechanical properties as well as their low cost. The FRP bars were sourced from MagmaTech Ltd [48] and Table 2 presents the mechanical properties according to [49].

Epoxy adhesives are commonly used as the filler for the NSM structures [14], as they exhibit excellent bond quality at the interfacial regions resulting in higher capacities [19, 50] and were therefore applied in this study. Epoxy adhesives have been reported to have higher and better gap-filling capacities compared to conventional adhesives [50]. Moreover, 2-part epoxy adhesives show better shrinkage properties as well possessing thixotropic qualities. Hence, 2-part epoxy thixotropic adhesives with a thickness of 2 mm between the wall of the grooved timber and the FRP are adopted herein. The epoxy resins were supplied by Rotafix Ltd [52] and the material properties as provided by the manufacturer are provided in Table 2, where the bong strength refers to the bond between the adhesive and the timber.

Table 2: Material properties.

Material	**Tensile strength (N/mm^2)**	**Compressive strength (N/mm^2)**	**Bond strength (N/mm^2)**	**Shear Strength (N/mm^2)**	**Modulus of Elasticity (N/mm^2)**
Timber	8.6	34.1	-	3.2	7763
Epoxy [39]	40	>60	6		3000
BFRP [41]	920	-	-		54000
GFRP [41]	682	-	-		67300

In this experiment, white spruce timber species was examined. The specimens were visually graded C16 structural timber. Material tests were carried out in order to obtain the main material properties. Before fabrication four samples were cut from each specimen for the characterisation of the moisture content, the density and the compressive strength according to [42]. The average mean density was found to be 436 kg/m^3 with a standard deviation of 0.073. The average moisture content was equal to 15.4% with a standard deviation of 0.156. The average ultimate compressive strength at direction parallel to the grain was equal to 34.1 N/mm^2 with a standard deviation of 0.153. Timber's material properties are also included in Table 2. Note that the tensile and shear strength correspond to characteristic values suggested by BS EN 384 [54] for C16 grade. The Young's modulus has been calculated on the basis of the experimental flexural rigidity (EI) values (see Section 4.4) of unreinforced beams.

3.2 Fabrication of NSM FRP timber specimens

A total of 20 timber beams were tested under four-point bending configuration until failure. All beams had a rectangular cross-section of 70×215 mm and were 2.5 m long. In design 1 (D1) configuration, the tensile zone of the beams was reinforced with two FRP bars (reinforcement percentage ρ equal to 0.67%), while in design 2 (D2), an additional bar was added in the compression zone (reinforcement percentage ρ equal to 1.0%). Two types of FRP bars, namely BFRP and GFRP, were considered. Four unreinforced timber beams (NR) were also tested for comparison purposes. The list of the tests along with their designation are summarised in Table 3. It is noted that each beam configuration was replicated 3 – 5 times. Similar replicates have been used by previous researchers such as [14], [18], [20].

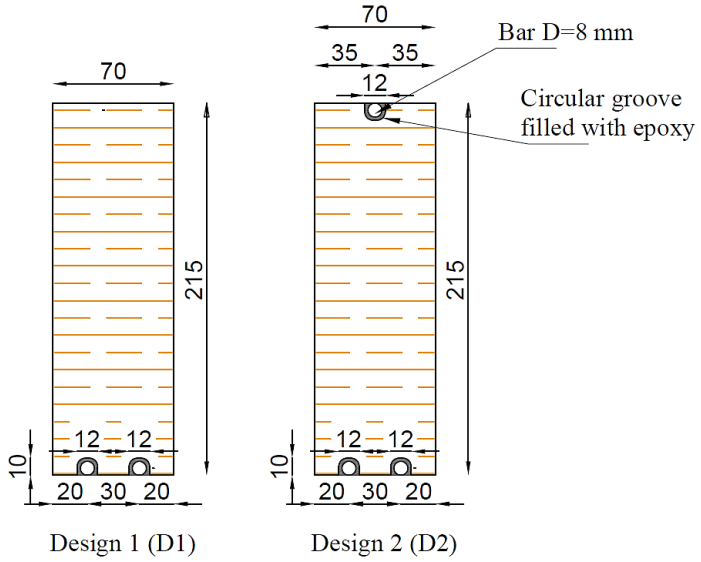

Figure 2: Configuration of reinforced beams (D1– bottom single reinforced with 2 bars in circular grooves; D2– bottom and top double reinforced with 2 and 1 bar respectively in circular grooves).

Table 3: List of timber beam specimens.

Reinforcement Type	Configuration	Replicates	Designation	Specimen Number
No reinforcement (NR)	N/A	4	NR - 1	B4
			NR - 2	B8
			NR - 3	B12
			NR - 4	B16
BFRP	D1	3	BFRP - D1 -1	B13
			BFRP - D1 -2	B14
			BFRP - D1 -3	B15
BFRP	D2	5	BFRP - D2 -1	B1
			BFRP - D2 -2	B2
			BFRP - D2 -3	B3
			BFRP - D2 -4	B19
			BFRP - D2 -5	B20
GFRP	D1	5	GFRP - D1 -1	B5
			GFRP - D1 -2	B6
			GFRP - D1 -3	B7
			GFRP - D1 -4	B17
			GFRP - D1 -5	B18
GFRP	D2	3	GFRP - D2 -1	B9
			GFRP - D2 -2	B10
			GFRP - D2 -3	B11

Figure 3 shows the fabrication process of the NSM FRP specimens. For the reinforced specimens, circular longitudinal grooves [33] were initially slotted at the considered locations (Step 2 at Figure 3a and Figure 3b). Prior to the bonding process, the slots were meticulously cleaned. The base and the hardener of the epoxy were thoroughly mixed with a mix ratio 1:0.4 for at least 3 minutes [52] until the material became smooth in consistency and uniform in colour. The epoxy resin was then applied to the length of the grooves (Step 3 at Figure 3a) and the FRP bars were inserted (Step 4 at Figure 3a and Figure 3c). Pressure was applied across the length of the reinforced beams to ensure adequate placement and bond between the adherents and the epoxy. A taping knife was used to ensure a level and uniform surface at the top of the beam. For D2 specimens, the bars on the tensile zone were initially placed, whilst the bar on the compression zone was bonded 24 hours later. The specimens were left for curing for 7 days before testing.

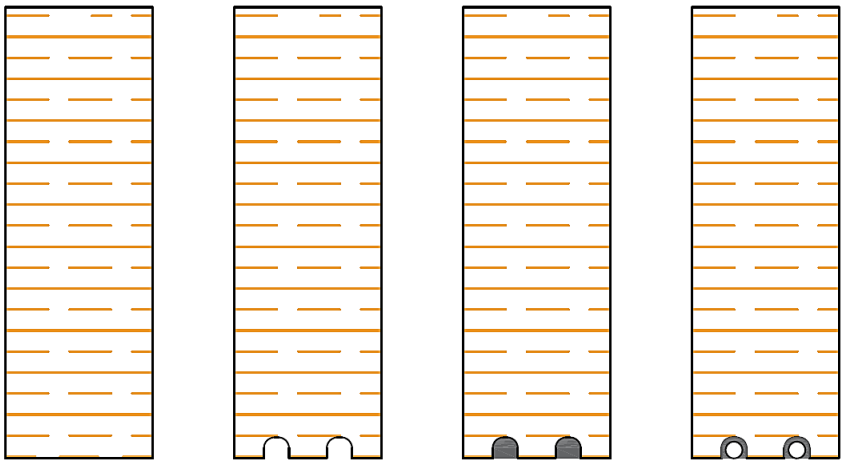

a) Fabrication process (D1)

b) Circular longitudinal grooves (Step 2)

c) Installed NSM FRP bar (Step 4)

Figure 3: Specimens preparation.

3.3 Test set-up

Figure 4 shows the test set-up of the timber beams. The specimens had a span of 2.3 m and were loaded with a hydraulic jack of 100 kN capacity. A preload of 300N [2] was initially applied. The type of the loading was displacement control quasi-static monotonic loading which was applied with a constant

rate of 3 mm/min [55] until the failure occurred. A load cell was used to record the applied load. The load was transferred to the specimen through an I-shaped steel spreader beam. Steel rollers and bearing plates were placed at the support points to allow load distribution and avoid local stress concentration. Linear variable displacement transducers (LVDTs) were placed at the mid-span to monitor the vertical displacement. Three strain gauges were attached at the mid-span along the depth of the beam (top, bottom and mid) in order to track the strain distribution profile. Data acquisition was automatically performed through a data logger system.

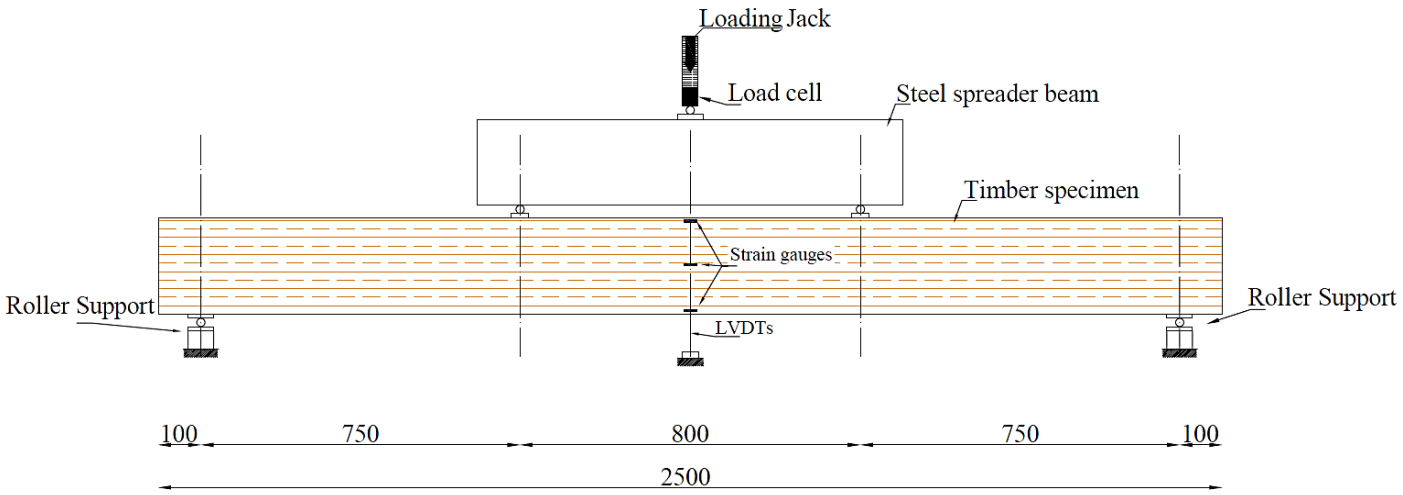

a) Schematic illustration

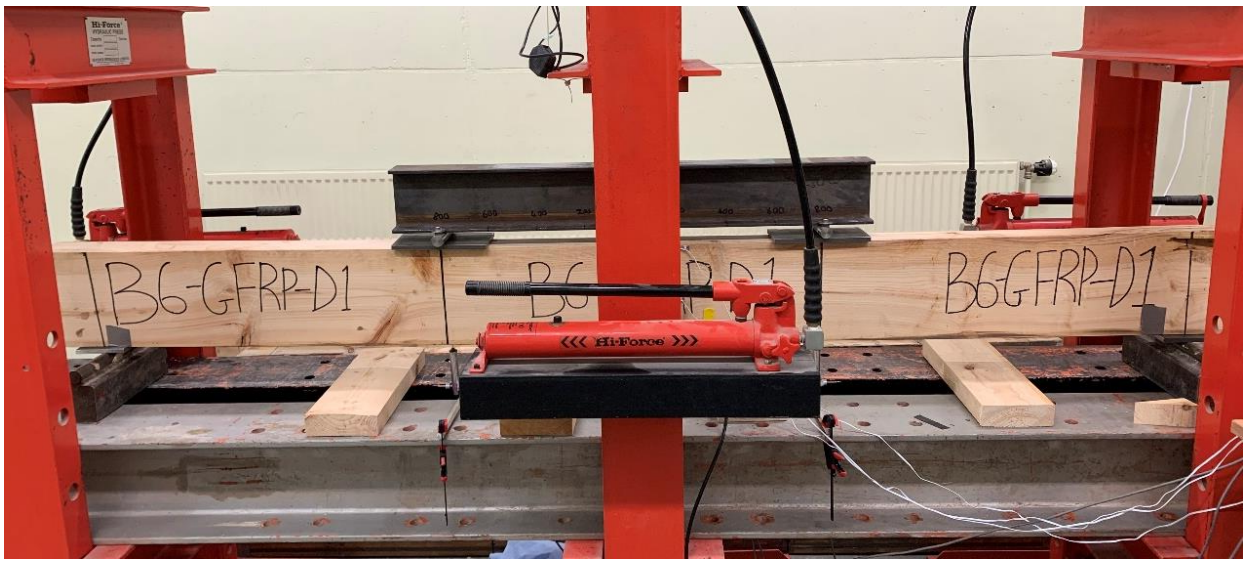

b) Photograph

Figure 4: Experimental set-up.

4. EXPERIMENTAL RESULTS AND DISCUSSION

4.1 Failure mode

In the present investigation, the overall or predominant failure mode for both reinforced and unreinforced beams was brittle tensile failure or splitting without compression failure in the compression zone. None of the FRP bars has failed and there was no cohesive failure observed for the epoxy adhesive. The visually observed failure modes were according to BS EN ISO 10365 [56]. Typical failure modes for all the beams are shown in Figure 5.

The unreinforced beams generally recorded brittle tensile behaviour at the tension zone. In most cases, the beams exhibited catastrophic failures. Unreinforced beam NR-1 (Figure 5a) exhibited cross-grained tension failure together with cracks at knots in the compression and tension zone. The failure was also accompanied with rupture at midspan. It is noteworthy that the examined timber contained juvenile wood at the depth of the beam as well as knots at the extreme fibres of the compression and tension zones. These defects were responsible for the premature failure of the beam. In both NR-2 and NR-3, there was rupture of wood due to brittle tension failure at the bottom tension zone. This was followed with horizontal splitting along the timber.

In specimens GFRP - D1 - 2, GFRP - D1 - 4, GFRP - D2 - 2, GFRP - D2 - 3, cracks were initiated and propagated around knots, as shown in Figure 5d. For three of the reinforced beams with FRP reinforcement with D2 configuration (BFRP - D2 - 2, BFRP - D2 - 4, GFRP - D2 -1), debonding between the bars and the timber was also observed at the tensile zone of the specimens at large displacements and after the attainment of the failure load, as shown in Figure 5e. Figure 6 presents the failed specimen GFRP - D2 -1, in which upon tensile failure, the crack on the central region of constant moment propagated up to the compressive zone, followed by bar debonding for even increasing deformation.

a) NR-1 (B4): tensile

b) BFRP - D1 - 1 (B13): tensile

c) BFRP - D1 - 2 (B14): tensile

d) GFRP - D1 - 4 (B17): tensile (initiated at knot)

e) BFRP - D2 - 4 (B19): tensile followed by debonding

f) GFRP - D2 - 4 (B11): tensile followed by debonding

Figure 5: Typical failure modes.

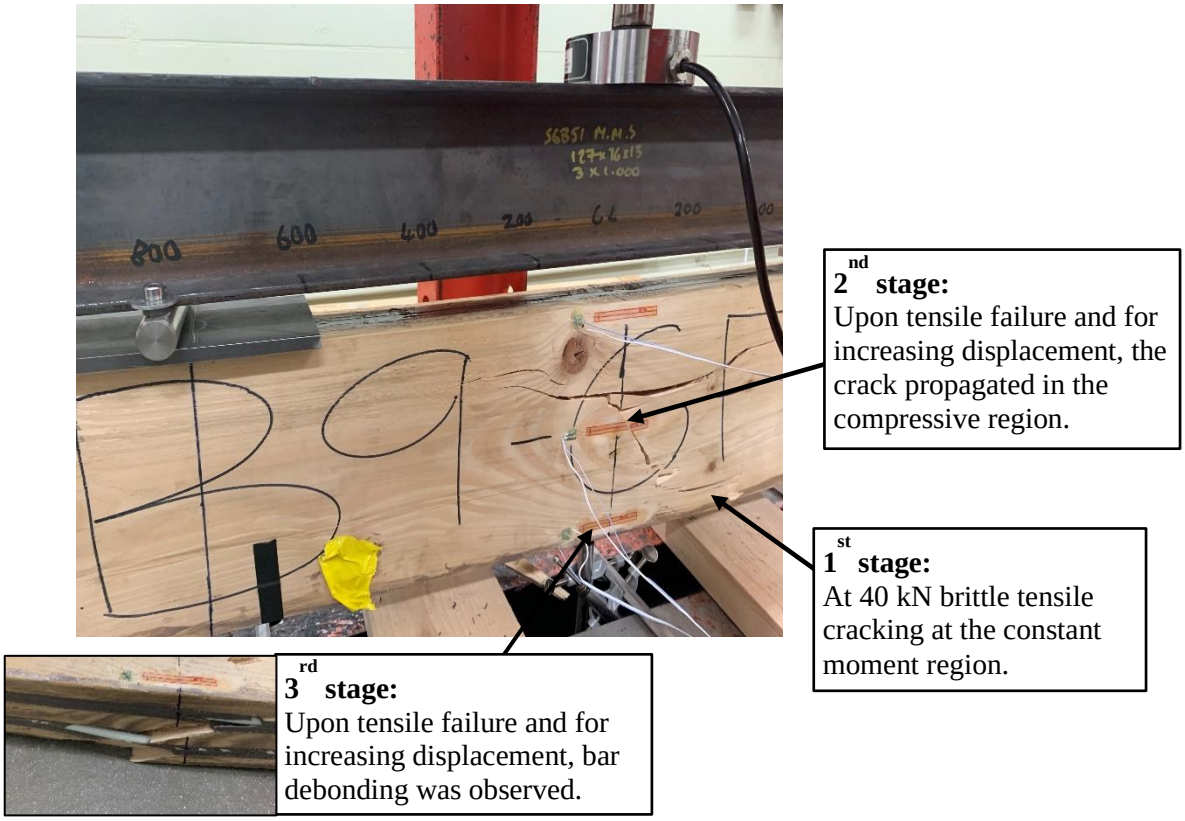

Figure 6: Failure mode of specimen GFRP - D2 -1 presented in stages.

4.2 Load-deflection curves and ultimate performance

Figure 7 shows the load versus mid-span vertical displacement curves for all tests. The maximum recorded load is considered as the failure load (N_u) which together with the failure moment M_u and the corresponding mid-span vertical displacements (δ_u) are listed in Table 4. Note that during testing, the applied load (N) was incrementally recorded. The incremental moment (M) of the central region of the statically determinate symmetric beam was evaluated by equation $M=(N/2)\times\alpha$ where α is the distance from the loading point to the support equal to 750 mm for this study.

As can be observed in Figure 7, the specimens indicated a linear response until brittle tensile failure. The ultimate load of the reinforced beams was significantly higher than that of the corresponding unreinforced ones. The same conclusion can be drawn for both BFRP and GFRP reinforced bars. Moreover, the displacement on which the ultimate performance was attached increased for the reinforced beams. As seen in Figure 7 and Table 4, there was a significant variation of ultimate load and moment capacity recorded among the unreinforced beams. The highest and lowest ultimate performance was recorded by NR-2 and NR-1, respectively. In particular, the recorded ultimate load of NR-2 is about 69% higher than that of NR-1. The NR-1 contained juvenile wood and cross-grain as

well as cluster of knots at extreme fibres of both the compression as well as tensile zone (see Figure 5a). These defects, it is believed, caused the timber to fail before reaching its full capacity. Moreover, according to Table 4, the biggest coefficient of variation (COV) in the ultimate performance has been found for NR beams, whilst the variability appears reduced at the reinforced compared to the unreinforced beams, as the FRP bars are capable of arresting crack openings and bridging timber defects. In particular, the smallest coefficient of variation (COV) on the achieved ultimate load has been observed for BFRP – D1 group followed by BFRP – D2 group.

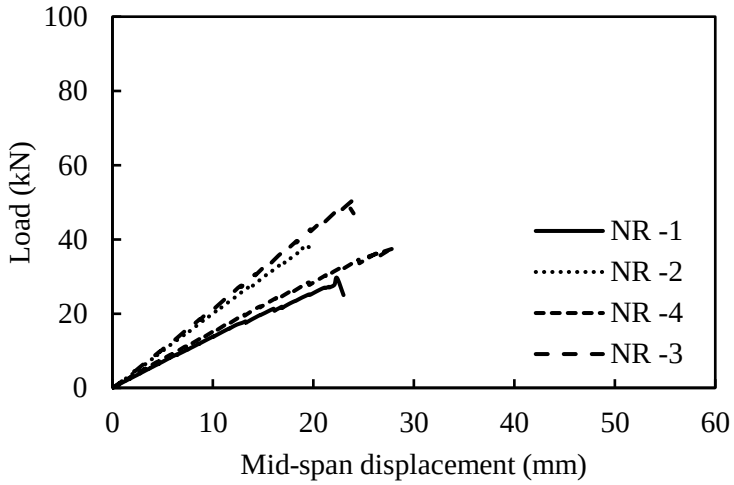

a) NR

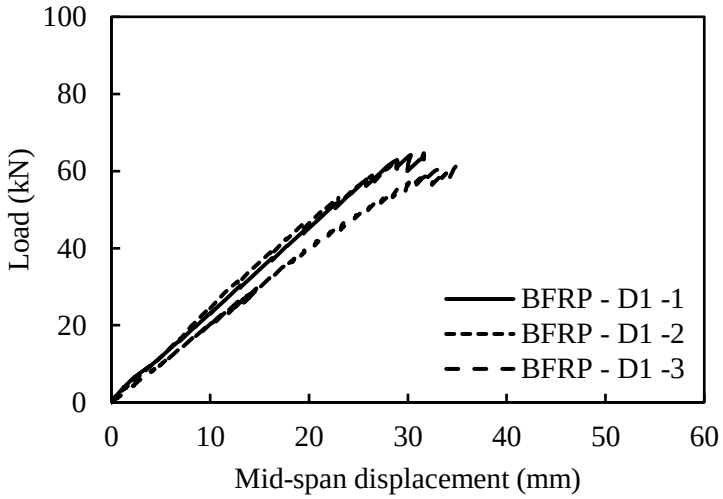

b) BFRP - D1

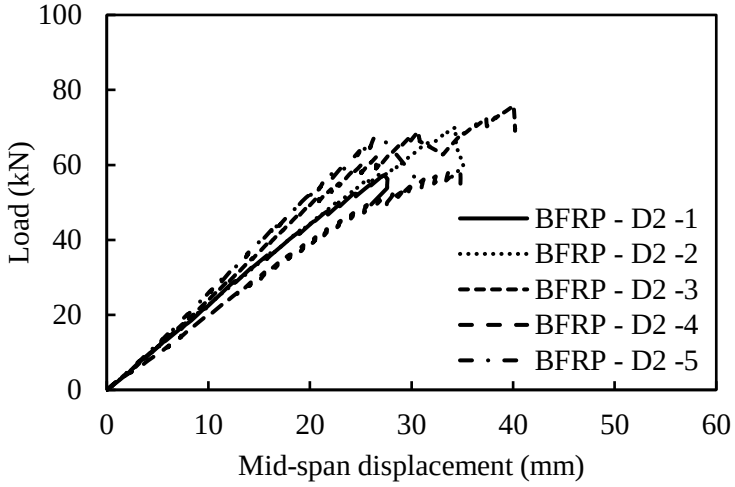

c) BFRP - D2

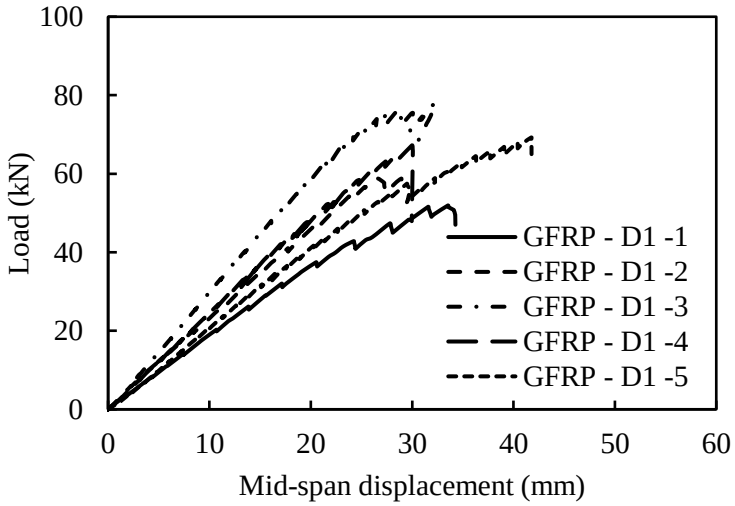

d) GFRP - D1

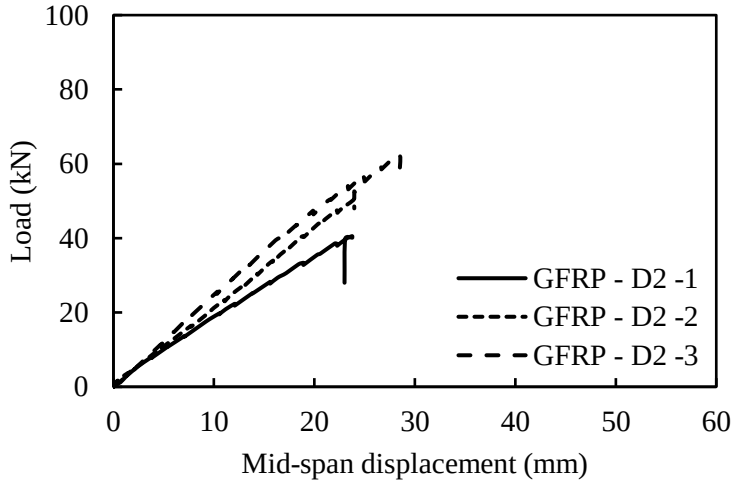

e) GFRP - D2

Figure 7: Load vs mid-span displacement curves.

Table 4: Failure loads (N_u), failure moments (M_u) and corresponding mid-span displacements (δ_u).

Designation	**Specimen Number**	**N_u (kN)**	**M_u (kNm)**	**δ_u (mm)**
NR - 1	B4	29.65	11.12	22.34
NR - 2	B8	50.26	18.85	23.79
NR - 3	B12	38.43	14.41	19.17
NR - 4	B16	37.54	14.08	27.94
	Average	38.97	14.61	23.31
	COV	0.22	0.22	0.16
BFRP - D1 -1	B13	64.64	24.24	31.62
BFRP - D1 -2	B14	62.75	23.53	28.90
BFRP - D1 -3	B15	61.63	23.11	34.96
	Average	63.01	23.63	31.82
	COV	0.02	0.02	0.10
BFRP - D2 -1	B1	57.32	21.50	27.37
BFRP - D2 -2	B2	69.99	26.25	34.34
BFRP - D2 -3	B3	75.74	28.40	40.91
BFRP - D2 -4	B19	58.35	21.88	34.67
BFRP - D2 -5	B20	67.60	25.35	26.84
	Average	65.80	24.66	32.66
	COV	0.12	0.12	0.17
GFRP - D1 -1	B5	51.94	19.48	33.54
GFRP - D1 -2	B6	58.88	22.08	26.34
GFRP - D1 -3	B7	77.97	29.24	32.35
GFRP - D1 -4	B17	67.25	25.22	29.98
GFRP - D1 -5	B18	69.27	25.98	41.76
	Average	65.06	24.40	32.79
	COV	0.15	0.15	0.17
GFRP - D2 -1	B9	40.55	15.21	23.76
GFRP - D2 -2	B10	52.54	19.70	23.97
GFRP - D2 -3	B11	62.61	23.48	28.55
	Average	51.90	19.47	25.43
	COV	0.21	0.15	0.11

4.3 Strain distribution profile

Load vs microstrain graphs across the cross-sectional depth (top, bottom and mid strain gauge values) have been evaluated and the typical strain distribution profiles across the cross-sectional depth are given in Figure 8. Overall, it can be seen that the plain section assumption which is the basis of elastic bending theory has been obeyed. For the reinforced beams, non-linear response can also be observed, while for some of the reinforced beams, the neutral axis seems to be slightly lowered which is in line with previous observations [33]. In addition, as can be seen, the strain gauges at the compression zone of GRFP - D2 - 3 recorded non-linear behaviour in comparison to the other GFRP members. This deviation is noticeable at higher loads, between 20 kN – 62 kN. As the load increased, there were cracks in a knot at the soffit in the tension zone of the beam. With increasing displacement, micro

cracking were noticeable and propagated in the compressive region at higher load level (see Figure 5f). It is probable that, the micro cracking at higher loads is responsible for such non-linearity at the compression zone of this specimen. Furthermore, on the basis of the recorded strain values and the obtained strain distribution profiles, the tensile strains at timber at ultimate load ($\varepsilon_{wtu,exp}$) have been evaluated for each beam. Average values for each data set are shown in Table 5. Using the modulus of Elasticity of FRPs, the corresponding tensile stresses of FRP ($\sigma_{f,exp}$) when timber failed are also reported in Table 5.

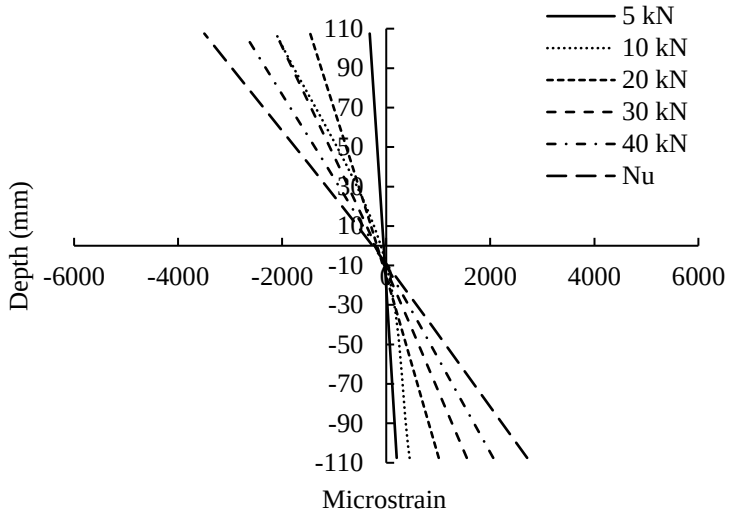

a) NR - 2 (B8)

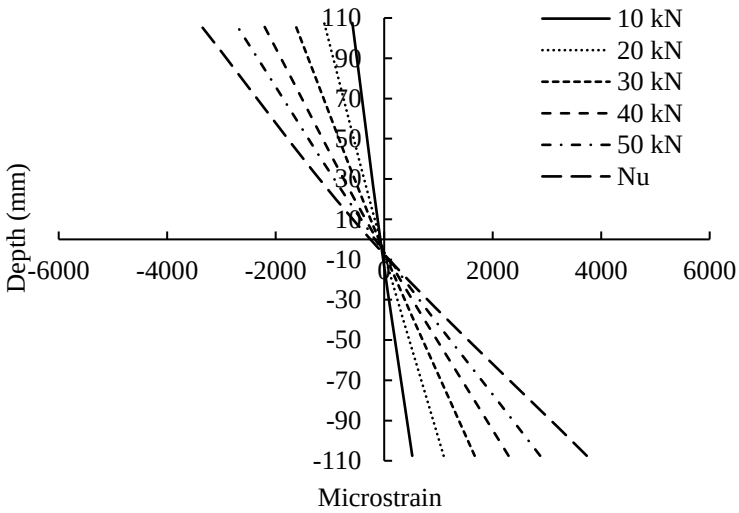

b) BFRP - D1 - 3 (B15)

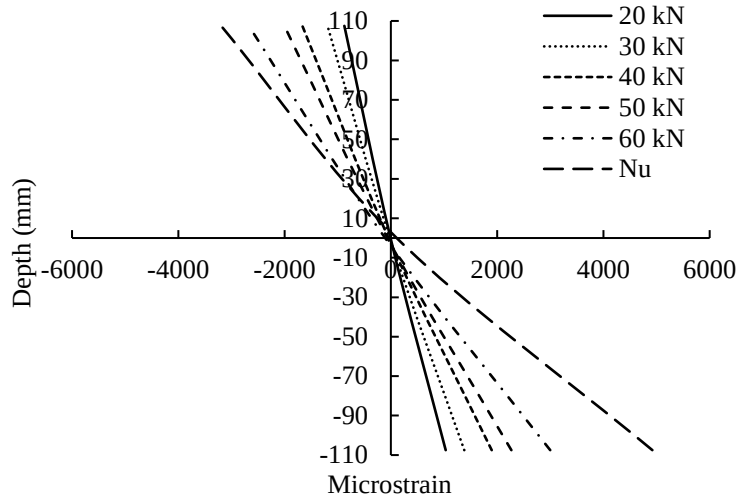

c) GFRP - D1 - 3 (B7)

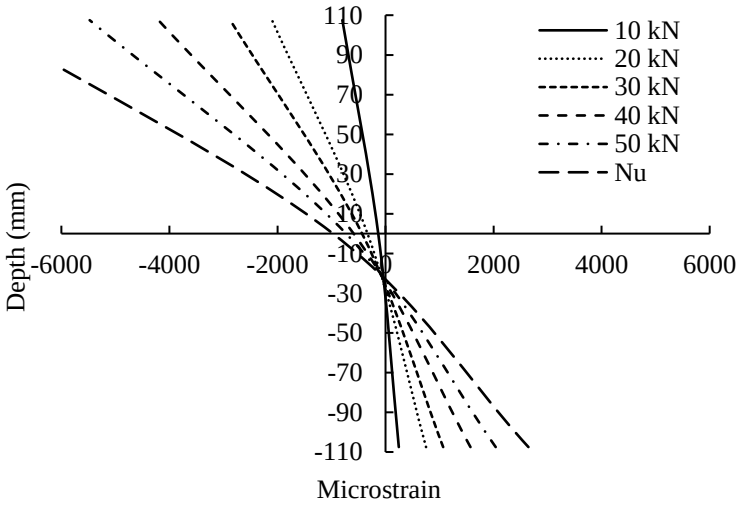

d) GRFP - D2 - 3 (B11)

Figure 8: Typical strain distribution profile of beams.

Table 5: Ultimate tensile strains ($\varepsilon_{tu,exp}$) and corresponding stresses of FRP ($\sigma_{f,exp}$) when timber failed.

Specimen	**Replicates**	**$\varepsilon_{tu,exp}$ (%)**	**$\sigma_{f,exp}$ (N/mm^2)**
NR	4	0.38	-
BFRP - D1	3	0.43	234
BFRP - D2	5	0.38	207
GFRP - D1	5	0.41	273
GFRP - D2	3	0.23	153

4.4 Comparison of stiffness and ultimate performance between examined configurations

The average ultimate loads and corresponding displacements for each group of specimens are summarised in Table 6. Using the general stiffness formulation, the global flexural rigidity (EI) and the stiffness values (k) of each beam can be calculated via Eq. (1):

$$\Delta P = k\Delta\delta = \frac{48EI}{\alpha(3L^2 - 4\alpha^2)}\Delta\delta \quad (1)$$

where ΔP is the range of the applied load and $\Delta\delta$ the corresponding range of the mid-span vertical displacement, E is the modulus of Elasticity, I is the second moment of area, L is the span of the beam, equal to 2300 mm herein and α is the distance from the loading point to the support.
Moreover, average values for the studied groups of the experimental global flexural rigidity (EI) values and the stiffness values ($k=\Delta P/\Delta\delta$) are also shown Table 6.

As can be observed, the reinforced beams generally achieved higher load, displacement and global flexural rigidity compared to the unreinforced ones (NR). In particular, the increase in the maximum load was in the range of 33%-69%, the increase of the displacement at failure was in the range of 9%-41% and the increase of the global flexural rigidity and stiffness in the range of 22%-33%. Similar response can be noted between GFRP-D1 and BFRP-D1 with a slightly higher average load in the case of GFRP. Overall, the reinforced beams presented an increase of 60% at the ultimate load, 34% at the mid-span displacement at failure and 30% at the flexural rigidity and stiffness compared to corresponding the control beams. Similar findings are also graphically shown in Figure 9, where average values of the stiffness, the ultimate loads and displacements with error bars for the standard deviations for each data set are presented.

Comparing the BFRP-D1 (two bars on the tension zone) with BFRP-D2 (two bars on the tension zone and one on the compression zone), only slightly increased performance can be observed for the latter. In the case of specimens reinforced with the glass fibres, the D1 specimens recorded higher loads and flexural stiffness in comparison with the corresponding D2 specimens. The lower performance of the GFRP-D2 specimens might be due to poor timber quality, in particular, for GFRP-D2-1 and GFRP-D2-2 specimens. Moreover, the grooving or machining of grooves for NSM fabrication might have caused the weakening of the timber (GFRP-D2-1 and GFRP-D2-2) specimens, which means a discontinuity was introduced into the timber fibres in the proximity of the groove [35].

It was observed that increasing the FRP reinforcement at the bottom (with two FRP bars) and the top (with one FRP bar) of the beams might not necessary improve the capacity of the NSM beams over

the corresponding ones with two FRPs reinforcement at bottom. In tensile-controlled beams like the ones studied herein, the ultimate load would have been possibly increased if in addition to the bar at the compression zone, the tensile reinforcement had been increased as well. It is noted that before increasing the cross-sectional area of the reinforcement, additional factors such as the distance between the adjacent grooves as well as edge distances of the timber beams should be considered [11].

Table 6: Average values of forces and displacements and comparison with non-reinforced timber beams.

Specimen	**Replicates**	**N_u (kN)**	**increase (%)**	**δ_u (mm)**	**increase (%)**	**EI (Nmm^2)**	**increase (%)**	**k (N/mm)**	**increase (%)**
NR	4	38.97	-	23.31	-	3.70E+11	-	1741	-
BFRP - D1	3	63.01	62%	31.82	37%	4.86E+11	31%	2283	31%
BFRP - D2	5	65.80	69%	32.66	40%	4.91E+11	33%	2309	33%
GFRP - D1	5	65.06	67%	32.79	41%	4.90E+11	32%	2305	32%
GFRP - D2	3	51.90	33%	25.43	9%	4.51E+11	22%	2121	22%
BFRP&GFRP-D1&D2	16	62.44	60%	31.19	34%	4.83E+11	30%	2268	30%

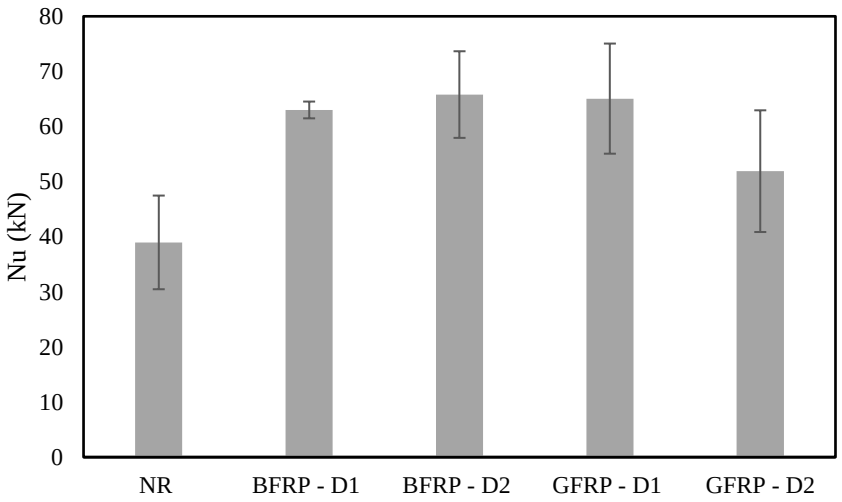

a) average ultimate load

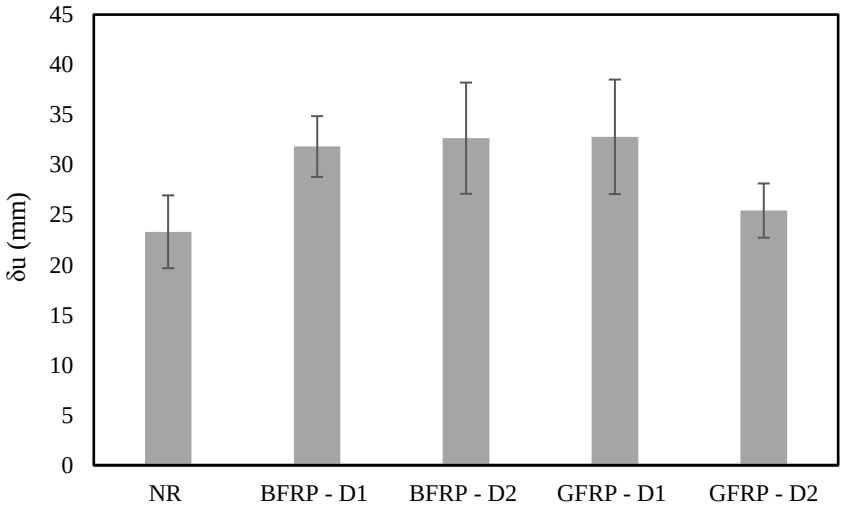

b) average displacement at ultimate load

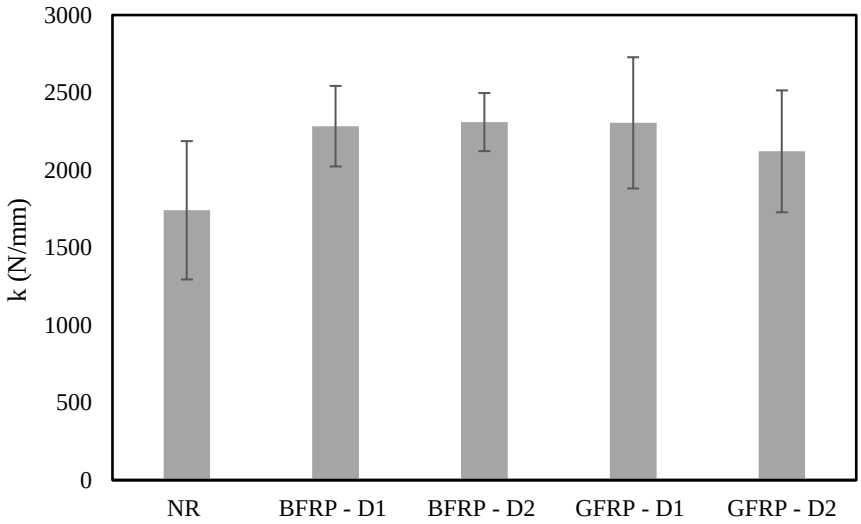

c) average stiffness

Figure 9: Graphical presentations of average values of ultimate load, displacement and stiffness.

5. THEORETICAL ANALYSIS

In absence of a standard method for the prediction of the NSM FRP timber flexural capacity, the present paper applies a general theoretical model in order to estimate the moment resistance of the NSM FRP timber beams. Basic constitutive laws for timber and FRP materials are used for the theoretical analysis. The applied stress (σ) – strain (ε) curves for both FRP bars and timber are shown in Figure 10. A linear elastic response is considered for the FRPs and for the tensile timber, while for the compressive behaviour of timber a bilinear curve is assumed according to [57]. In Figure 10, E is the modulus of Elasticity, f is the strength, whilst the subscripts f and w correspond to FRP and timber, the subscripts t and c to tension and compression and the subscripts u and y to ultimate and yield state, respectively.

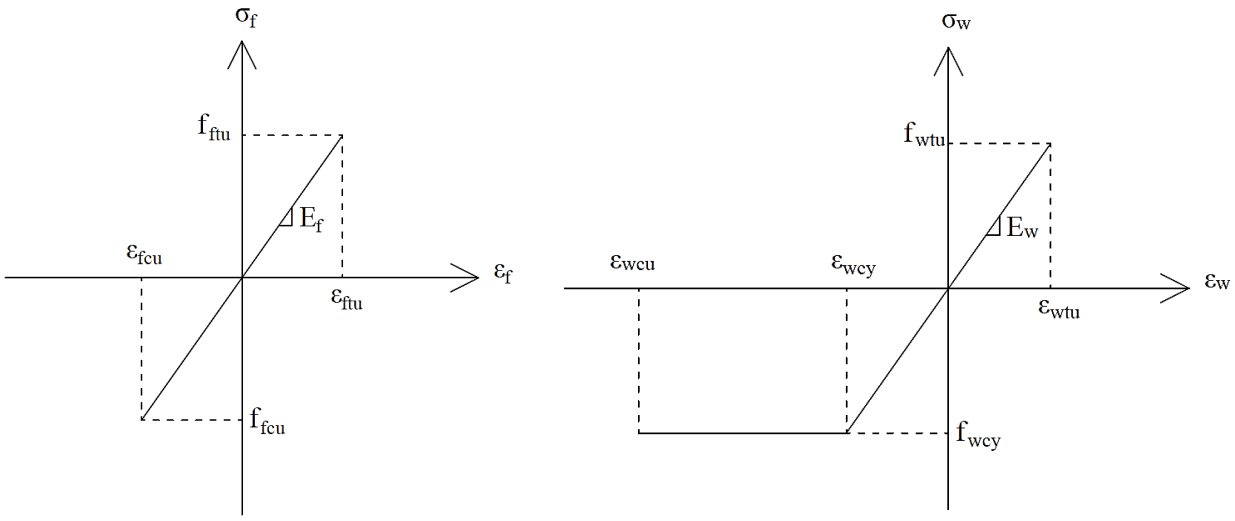

a) Stress-strain of FRP b) Stress-strain of timber

Figure 10: Constitutive material laws for theoretical analysis.

Focus of this paper has been placed upon the flexural response, hence the model was based on pure bending theory and plain section assumption, whilst debonding between bars and timber and long-term phenomena, like creep and fatigue have not been considered. In line with the experimental findings, timber tensile failure was considered as the main failure mode. The equilibrium of the reinforced beam cross-section for both considered configurations are shown in Figure 11, where F stands for the force of the subscript, as previously defined. Moreover, x_c and x_t are the depth of the compression and the tension zone, respectively, while x_c is divided in x_{c1} and x_{c2} for the timber part in plastic and elastic region, respectively. In addition, z_{ft} and z_{fc} is the distance of the centre of the FRP bars from the beam's

edge for the tensile and compression bars, respectively. The ultimate theoretical moment ($M_{u,theor}$) can be calculated from Eq. (2)

$$M_{u,theor} = F_{wc1}(x_c - \frac{1}{2}x_{c1}) + \frac{2}{3}F_{wc2}\,x_{c2} + F_{fc}(x_c - z_{fc}) + \frac{2}{3}F_{wt}\,x_t + F_{ft}(x_t - z_{ft}) = \quad (2)$$

$$bf_{wcy}\,x_{c1}(x_c - \frac{1}{2}x_{c1}) + \frac{1}{3}bf_{wcy}\,x_{c2}^{\,2} + f_{wcy}\frac{E_f}{E_w}A_{fc}(x_c - z_{fc}) + \frac{1}{3}bf_{wtu}\,x_t^{\,2} + f_{wtu}\frac{E_f}{E_w}A_{ft}(x_t - z_{ft})$$

Where A_{ft} and A_{fc} the cross-sectional areas of the FRP bars at the tensile and compression zone respectively. Note that F_{fc} is zero for D1 beams of the present study (Figure 11a).

In order to evaluate the ultimate moment resistance, the values of x_c, x_{c1}, x_{c2} and x_t should be calculated. These four unknowns are computed following principles of geometry (Eqs. (3) and (4)), trigonometry (Eq. (5)) and equilibrium of forces (Eq. (6)).

$$x_c + x_t = h \quad (3)$$

$$x_{c1} + x_{c2} = x_c \quad (4)$$

$$\frac{x_t}{x_{c2}} = \frac{\varepsilon_{wtu}}{\varepsilon_{wcy}} \quad (5)$$

$$F_{wc1} + F_{wc2} + F_{fc} = F_{ft} + F_{wt} \rightarrow$$

$$bf_{wcy}x_{c1} + \frac{1}{2}bf_{wcy}x_{c2} + f_{wcy}\frac{E_f}{E_w}A_{fc} = \frac{1}{2}bf_{wtu}x_t + f_{wtu}\frac{E_f}{E_w}A_{ft} \quad (6)$$

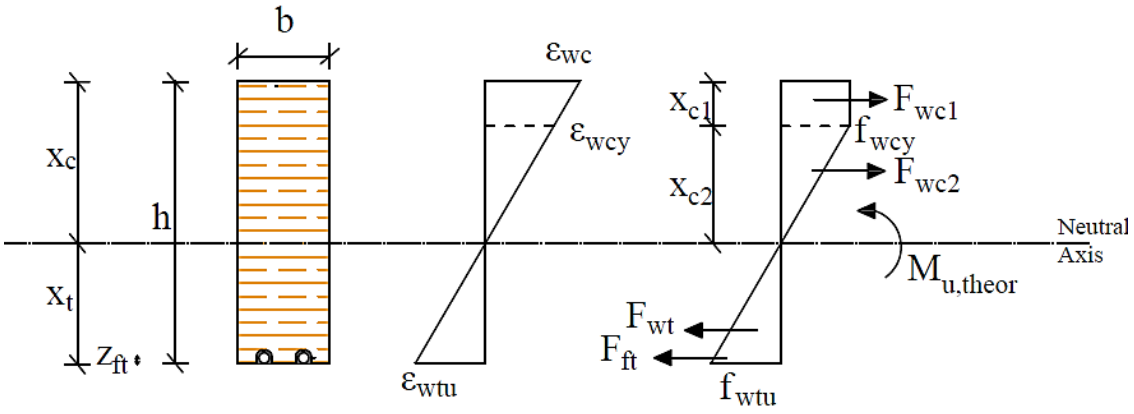

a) Configuration D1

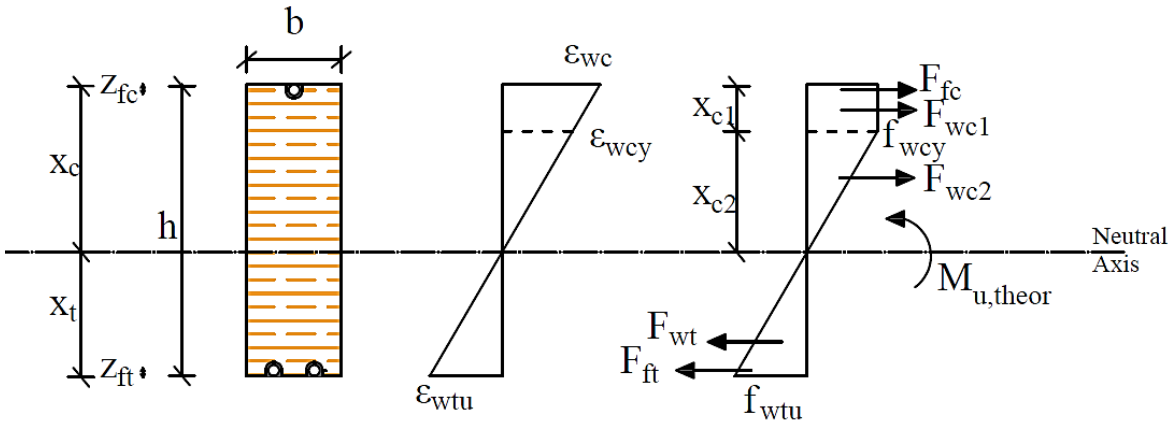

b) Configuration D2

Figure 11: Equilibrium of the reinforced beam cross-section for both considered configurations.

Using Eqs. (2)-(6), the material laws shown in Figure 10, the Moduli of Elasticity of timber, BFRP and GFRP shown in Table 2, and the ultimate tensile strain values obtained from NR beams according to Table 5, the theoretical moment resistance ($M_{u,theor}$) and the corresponding force ($F_{u,theor}$) have been evaluated. It is noteworthy that for all the examined beams, x_{c1} was found equal to zero and hence the compressive part of the timber was under elastic state and the failure occurred when timber reached the ultimate tensile strain, which was in line with experimental observations. Applying Eq. (1), the experimental and theoretical stiffness values have also been calculated and are presented in Table 7, showing a fair comparison. Given that for the examined beams, a linear response was primarily noted until a failure, a comparison can be made between the displacement ($\delta_{u,exp}$) at which the ultimate load was attained and the theoretical displacement ($\delta_{u,theor}$) calculated from Eq. (1) for ΔP equal to $F_{u,theor}$, i.e. considering a linear response in the structure. It can be seen that experimental displacements are underestimated by 39% on average compared to the theoretical linear predictions.

The theoretical moment resistance ($M_{u,theor}$) for the studied beams are compared with the experimental values ($M_{u,exp}$). The comparison is presented in Table 7, where it can be seen an average ratio of $M_{u,exp}/M_{u,theor}$ equal to 1.09, showing that the ultimate theoretical predictions are in good comparison with experimental ones. A graphical comparison between the experimental and theoretical results is also shown in Figure 12. Collated data from [14] and [16] have also been included demonstrating further the applicability of the proposed equations.

Table 7: Comparison between experimental and theoretical predictions.

Specimen	k_{exp} (N/mm)	k_{theor} (N/mm)	k_{exp} /k_{theor}	$\delta_{u,exp}$ (mm)	δ_{theor} (mm)	$\delta_{u,exp}$/ δ_{theor}	$M_{u,exp}$ (kNm)	$M_{u,theor}$ (kNm)	$M_{u,exp}$/ $M_{u,theor}$
NR-1	1281	2120	0.60	22.34	20.94	1.07	11.12	17.37	0.64
NR-2	2222	2120	1.05	23.79	20.94	1.14	18.85	17.37	1.09
NR-3	2007	2120	0.95	19.17	20.94	0.92	14.41	17.37	0.83
NR-4	1452	2120	0.68	27.94	20.94	1.33	14.08	17.37	0.81
BFRP - D1 -1	2238	2410	0.93	31.62	20.74	1.52	24.24	19.55	1.24
BFRP - D1 -2	2563	2410	1.06	28.90	20.74	1.39	23.53	19.55	1.20
BFRP - D1 -3	2049	2410	0.85	34.96	20.74	1.69	23.11	19.55	1.18
BFRP - D2 -1	2213	2411	0.92	27.37	22.04	1.24	21.50	20.78	1.03
BFRP - D2 -2	2304	2411	0.96	34.34	22.04	1.56	26.25	20.78	1.26
BFRP - D2 -3	2414	2411	1.00	40.06	22.04	1.82	28.40	20.78	1.37
BFRP - D2 -4	2064	2411	0.86	34.67	22.04	1.57	21.88	20.78	1.05
BFRP - D2 -5	2554	2411	1.06	26.84	22.04	1.22	25.35	20.78	1.22
GFRP - D1 -1	1828	2484	0.74	33.54	20.67	1.62	19.48	20.07	0.97
GFRP - D1 -2	2138	2484	0.86	26.34	20.67	1.27	22.08	20.07	1.10
GFRP - D1 -3	2942	2484	1.18	32.35	20.67	1.57	29.24	20.07	1.46
GFRP - D1 -4	2475	2484	1.00	29.98	20.67	1.45	25.22	20.07	1.26
GFRP - D1 -5	2139	2484	0.86	41.76	20.67	2.02	25.98	20.07	1.29
GFRP - D2 -1	1755	2488	0.71	23.76	22.22	1.07	15.21	21.62	0.70
GFRP - D2 -2	2071	2488	0.83	23.97	22.22	1.08	19.70	21.62	0.91
GFRP - D2 -3	2537	2488	1.02	28.55	22.22	1.29	23.48	21.62	1.09
		Mean	0.91		Mean	1.39		Mean	1.09
		COV	0.16		COV	0.20		COV	0.20

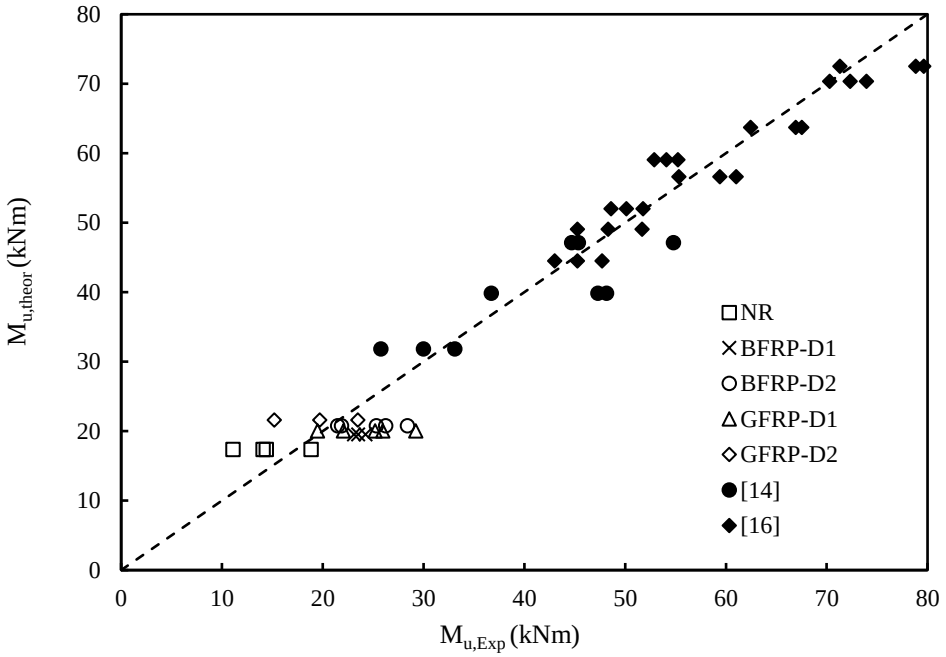

Figure 12: Graphical comparison between experimental and theoretical results on the basis of this study and collated data.

6. CONCLUSIONS AND FUTURE RECOMMENDATIONS

The paper reports an experimental study of white spruce timber beams reinforced with BFRP and GFRP bars with NSM technique. A series of 20 beams were tested under displacement control quasi-static monotonic loading. The obtained results led to the following conclusions:

(1) Reinforcing timber beams with NSM FRP bars is an efficient way of increasing both the stiffness and the ultimate capacity of flexural timber members. In particular, the percentage increase of the ultimate load and the flexural stiffness were within the range of 33%-69% and 22%-39%, respectively.

(2) The mid-span displacement at failure was also increased by 34% on average for the reinforced beams compared to the control beams.

(3) The predominant observed failure mode for both the unreinforced and the NSM FRP reinforced beams was brittle tensile failure of the timber at the tensile zone.

(4) The BFRP and GFRP reinforcement reduced the variability on the ultimate performance of the NSM FRP beams compared to the unreinforced beams.

(5) Increasing the FRP reinforcement at the bottom (with two FRP bars) and the top (with one FRP bar) of the beams did not significantly improve the capacity and behaviour of the NSM beams over the corresponding ones with two FRP bars reinforcement at bottom.

(6) Theoretical predictions of the ultimate flexural performance were presented and found to have an average $M_{u,exp}/M_{u,theor}$ equal to 1.09. The proposed formulae have also been assessed on the basis of collated data showing a good comparison.

It is noted that limitations of the current study included the number of test replicates. In view of the present study, the following suggestions are made for future research:

(1) More NSM FRP timber beams should be replicated and tested to account for heterogeneity of timber.

(2) Investigation of the tension and compression cross-sectional area of the reinforcement for optimum mechanical properties of NSM timber members. The proposed theoretical formulae proposed in this study can be applied in this process.

(3) Finite element analysis should be considered for clear understanding of flexural and bond behaviour of NSM in timber.

(4) Further to flexural testing, more pull-out specimens with different configurations should be tested to characterise and understand various factors influencing NSM FRP timber structures.

Acknowledgements

The authors are grateful to the technicians of the School of Civil Engineering and Built Environment of Liverpool John Moores University for their valuable assistance. In addition, the financial support of the Faculty of Engineering and Technology of Liverpool John Moores University is gratefully acknowledged.

REFERENCES

[1] Harte, A. and Crews, K. (2015) Reinforcement of timber structures. Construction and Building Materials, 97, pp.1-130.

[2] Raftery, G.M. and Kelly, F. (2015) 'Basalt FRP rods for reinforcement and repair of timber', Composites Part B: Engineering, 70, pp. 9–19. doi: 10.1016/j.compositesb.2014.10.036.

[3] Usman, A.P. and Sugiri, S. (2015) 'Analysis of the strength of timber and glulam timber beams with steel reinforcement', Journal of Engineering and Technological Sciences, 47(6), pp. 601–611. doi: 10.5614/j.eng.technol.sci.2015.47.6.1.

[4] Yusof, A. (2013) 'Ductility of Timber Beams Strengthened Using Fiber Reinforced Polymer', Journal of Civil Engineering and Architecture, 7(5), pp. 535–544. doi: 10.17265/1934-7359/2013.05.003.

[5] Amran, Y. M., Alyousef, R., Rashid, R. S., Alabduljabbar, H., and Hung, C. C. (2018) 'Properties and applications of FRP in strengthening RC structures: A review' Structures, 16, pp. 208–238. doi: 10.1016/j.istruc.2018.09.008

[6] Sonnenschein, R., Gajdosova, K. and Holly, I. (2016) 'FRP Composites and their Using in the Construction of Bridges', Procedia Engineering, 161, pp. 477–482. doi: 10.1016/j.proeng.2016.08.665.

[7] Fiorelli, J. and Dias, A.A. (2011) 'Glulam beams reinforced with FRP externally-bonded: theoretical and experimental evaluation. Materials and Structures', 44(8), pp.1431–1440. doi: 10.1617/s11527-011-9708-y

[8] Corradi, M., Vo, T.P., Pologanathan, K. and Osofero, A.I. (2021) Flexural behaviour of hardwood and softwood beams with mechanically connected GFRP plates. Composite Structures, 206, pp.610-620.

[9] Ling, Z., Liu, W. and Shao, J. (2020) Experimental and theoretical investigation on shear behaviour of small-scale timber beams strengthened with Fiber-Reinforced Polymer composites. Composite Structures, 240, p.111989.

[10] Jung, W.T., Park, J.S., Kang, J.Y. and Keum, M.S. (2017) Flexural behavior of concrete beam

strengthened by near-surface mounted CFRP reinforcement using equivalent section model. Advances in Materials Science and Engineering

[11] De Lorenzis, L. and Teng, J. G. (2007) 'Near-surface mounted FRP reinforcement: An emerging technique for strengthening structures', Composites Part B: Engineering, 38(2), pp. 119–143. doi: 10.1016/j.compositesb.2006.08.003.

[12] Szabó, Z.K. and Balázs, G.L. (2007) 'Near surface mounted FRP reinforcement for strengthening of concrete structures', Periodica Polytechnica Civil Engineering, 51(1), pp. 33–38. doi: 10.3311/pp.ci.2007-1.05.

[13] Poletti, E., Vasconcelos, G. and Jorge, M. (2015) Application of near surface mounted (NSM) strengthening technique to traditional timber frame walls. Construction and Building Materials, 76, pp.34-50.

[14] Johnsson, H., Blanksvärd, T. and Carolin, A. (2007) 'Glulam members strengthened by carbon fibre reinforcement', Materials and Structures, 40(1), pp. 47–56. doi: 10.1617/s11527-006-9119-7.

[15] Gentile, C., Svecova, D. and Rizkalla, S. H. (2002) 'Timber beams strengthened with GFRP bars: Development and applications', Journal of Composites for Construction, 6(1), pp. 11–20. doi: 10.1061/(ASCE)1090-0268(2002)6:1(11).

[16] Lu, W., Ling, Z., Geng, Q., Liu, W., Yang, H. and Yue, K. (2015) 'Study on flexural behaviour of glulam beams reinforced by Near Surface Mounted (NSM) CFRP laminates', Construction and Building Materials, 91, pp.23–31. doi: 10.1016/j.conbuildmat.2015.04.050

[17] Raftery, G.M. and Rodd, P.D. (2015) 'FRP reinforcement of low-grade glulam timber bonded with wood adhesive', Construction and Building Materials, 91, pp. 116–125. doi: 10.1016/j.conbuildmat.2015.05.026.

[18] Xu, Q., Chen, L., Harries, K.A., Zhang, F., Wang, Z. and Chen, X.M. (2017) 'Experimental study and numerical simulation of long-term behavior of timber beams strengthened with near surface mounted CFRP bars', Materials and Structures, 50(1), pp. 1–13. doi: 10.1617/s11527-016-0874-9.

[19] Yang, H. Liu, W., Lu, W., Zhu, S. and Geng, O. (2016) 'Flexural behavior of FRP and steel reinforced glulam beams: Experimental and theoretical evaluation', Construction and Building Materials, 106, pp. 550–563. doi: 10.1016/j.conbuildmat.2015.12.135.

[20] Xueyu, X., Yiqingi, W., Rongjun, X. and Xuanxing, L. (2018) 'Experimental Study and Theoretical Analysis on Flexural Mechanical Properties of Reinforced Timber Beams', Advanced Composites Letters, 27(1), pp. 23–33. doi: 10.1177/096369351802700103.

[21] Cóias, V. (2007) Structural Rehabilitation of Ancient Buildings (in Portuguese).

[22] Tuakta, C. (2005) 'Use of Fiber Reinforced Polymer Composite in Bridge Structures', Doctoral dissertation, Massachusetts Institute of Technology.

[23] Karataş, M.A. and Gökkaya, H. (2018) 'A review on machinability of carbon fiber reinforced polymer (CFRP) and glass fiber reinforced polymer (GFRP) composite materials', Defence Technology, 14(4), pp. 318–326. doi: 10.1016/j.dt.2018.02.001.

[24] Schober, K.U., Harte, A.M., Kliger, R., Jockwer, R., Xu, Q. and Chen, J.F. (2015) 'FRP reinforcement of timber structures', Construction and Building Materials, 97, pp. 106–118. doi: 10.1016/j.conbuildmat.2015.06.020.

[25] Elanchezhian, C., Ramnath, B.V. and Hemalatha, J. (2014) 'Mechanical Behaviour of Glass and Carbon Fibre Reinforced Composites at Varying Strain Rates and Temperatures', Procedia Materials Science, 6, pp. 1405–1418. doi: 10.1016/j.mspro.2014.07.120.

[26] Benmokrane, B., El-Salakawy, E., El-Gamal, S. and Goulet, S. (2007) 'Construction and testing of an innovative concrete bridge deck totally reinforced with glass FRP bars: Val-Alain Bridge on Highway 20 East', Journal of Bridge Engineering, 12(5), pp.632–645. doi: 10.1061/(ASCE)1084-0702(2007)12:5(632)

[27] Smits, J. (2016) 'Fiber-Reinforced Polymer Bridge Design in the Netherlands: Architectural Challenges toward Innovative, Sustainable, and Durable Bridges', Engineering, 2(4), pp. 518–527. doi: 10.1016/J.ENG.2016.04.004.

[28] Fernando, D., Frangi, A. and Kobel, P. (2016) 'Behaviour of basalt fibre reinforced polymer strengthened timber laminates under tensile loading', Engineering Structures, 117, pp. 437–456. doi: 10.1016/j.engstruct.2016.03.009.

[29] Kumbhar, V. (2014) 'An Overview: Basalt Rock Fibers-New Construction Material', Acta Engineering International, 2(1), pp. 11–18.

[30] Täljsten, B., Carolin, A. and Nordin, H. (2003) Concrete structures strengthened with near surface mounted reinforcement of CFRP. Advances in structural engineering, 6(3), pp.201–213. doi: 10.1260/136943303322419223

[31] Steiger, R. Serrano, E., Stepinac, M., Rajcic, V., O'Neill, C., McPolin, D. and Widmann, R. (2015) 'Strengthening of timber structures with glued-in rods', Construction and Building Materials, 97, pp. 90–105. doi: 10.1016/j.conbuildmat.2015.03.097.

[32] Fiorelli, J. and Dias, A.A. (2006) 'Fiberglass-reinforced glulam beams: Mechanical properties and theoretical model', Materials Research, 9(3), pp. 263–269. doi: 10.1590/S1516-14392006000300004.

[33] Raftery, G.M. and Whelan, C. (2014) 'Low-grade glued laminated timber beams reinforced using improved arrangements of bonded-in GFRP rods', Construction and Building Materials, 52, pp. 209–220. doi: 10.1016/j.conbuildmat.2013.11.044.

[34] Banea, M. D. and Da Silva, L. F. M. (2009) 'Adhesively bonded joints in composite materials:

An overview', Proceedings of the Institution of Mechanical Engineers, Part L: Journal of Materials: Design and Applications, 223(1), pp. 1–18. doi: 10.1243/14644207JMDA219.

[35] Franke, S., Franke, B. and Harte, A. (2015) 'Failure modes and reinforcement techniques for timber beams–State of the art.' Construction and Building Materials, 97, pp.2-13.

[36] Chun, Q., Van Balen, K. and Pan, J. (2016) 'Flexural Performance of Small Fir and Pine Timber Beams Strengthened With Near-Surface Mounted Carbon-Fiber-Reinforced Polymer (NSM CFRP) Plates and Rods', International Journal of Architectural Heritage, 10(1), pp. 106–117. doi: 10.1080/15583058.2014.971195.

[37] Yeboah, D., Taylor, S. and McPolin, D. (2016) 'Experimental study of interfacial stress distribution of bonded-in BFRP rod glulam joints using fibre optic sensors (FOS)' Structures, 8, 53–62. doi: 10.1016/j.istruc.2016.08.006.

[38] Sena-Cruz, J.M., Barros, J.A., Coelho, M.R. and Silva, L.F. (2012) 'Efficiency of different techniques in flexural strengthening of RC beams under monotonic and fatigue loading' Construction and Building Materials, 29, pp. 175-82. doi: 10.1016/j.conbuildmat.2011.10.044

[39] Novidis, D.G. and Pantazopoulou, S.J. (2008) 'Bond tests of short NSM-FRP and steel bar anchorages', Journal of Composites for Construction, 12(3), pp. 323–333. doi: 10.1061/(ASCE)1090-0268(2008)12:3(323).

[40] Micelli, F. and De Lorenzis, L. (2013) 'Near-surface mounted flexural strengthening of reinforced concrete beams with low concrete strength', Proceedings of Institution of Civil Engineers: Construction Materials, 166(5), pp. 295–303. doi: 10.1680/coma.11.00056.

[41] Zhang, P., Hu, Y., Pang, Y., Feng, H., Gao, D., Zhao, J. and Sheikh, S.A. (2020) 'Influence factors analysis of the interfacial bond behavior between GFRP plates, concrete', Structures, 26, pp. 79–91.

[42] De Lorenzis L. (2002) Strengthening of RC structures with near surface mounted FRP rods. PhD Thesis, Department of Innovation Engineering, University of Lecce, Italy.

[43] Kliger, R., Johansson, M. and Crocetti, R. (2008) 'Strengthening timber with CFRP or steel plates - Short and long-term performance', 10th World Conference on Timber Engineering 2008, 1(January), pp. 414–421.

[44] Bakalarz, M.M., Kossakowski, P.G. and Tworzewski, P. (2020). Strengthening of Bent LVL Beams with Near-Surface Mounted (NSM) FRP Reinforcement. Materials, 13(10), p.2350.

[45] Kumbhar, V.P. (2014) An overview: basalt rock fibers-new construction material. Acta Engineering International, 2(1), pp.11-18.

[46] Maxineasa, S. G. and Taranu, N. (2018) Life cycle analysis of strengthening concrete beams with FRP, Eco-efficient Repair and Rehabilitation of Concrete Infrastructures. Elsevier Ltd. doi: 10.1016/B978-0-08-102181-1.00024-1.

[47] Hanafi, M., Aydin, E. and Ekinci, A. (2020) 'Engineering properties of basalt fiber-reinforced bottom ash cement paste composites', Materials, 13(8), pp. 1–15. doi: 10.3390/MA13081952.
[48] Magmatech.co.uk (2020) Magmatech. [online] Available at: <http://magmatech.co.uk> [Accessed 4 October 2020].
[49] Tharmarajah, G., Taylor, S., Robinson, D. and Cleland, D. (2010). Composite reinforcement for bridge deck slabs. Belfast, UK: Queen's University Belfast (QUB). pp2.
[50] De Lorenzis, L., Stratford, T.J. and Hollaway, L.C. (2008) 'Structurally deficient civil engineering infrastructure: Concrete, metallic, masonry and timber structures' Strengthening and Rehabilitation of Civil Infrastructures Using Fibre-Reinforced Polymer (FRP) Composites. Woodhead Publishing Limited. doi: 10.1533/9781845694890.1.
[51] Davis, G. (1997) 'The performance of adhesive systems for structural timbers', International Journal of Adhesion and Adhesives, 17(3), pp. 247–255. doi: 10.1016/S0143-7496(97)00010-9.
[52] Rotafix (2020) Rotafix Manufacturer Structural Adhesive, Cements And Coatings. [online] Available at: < https://rotafix.co.uk/products/timber-engineering/rotafix-engineering-adhesive/> [Accessed 4 October 2020].
[53] BS EN 408:2010+A1:2012 (2012) Timber structures-Structural timber and glued laminated timber-Determination of some physical and mechanical properties. British Standards Institution (BSI). London, UK.
[54] BS EN 384: 2016+A1:2018 (2018) Structural timber – determination of characteristic values of mechanical properties and density, British Standards Institution, London, UK
[55] Alhayek, H. and Svecova, D., 2012. Flexural stiffness and strength of GFRP-reinforced timber beams. Journal of composites for construction, 16(3), pp.245-252. doi: 10.1061/(ASCE)CC.1943-5614.0000261
[56] BS EN ISO 10365 (1995) 20/30414673 DC. Adhesives—designation of main failure patterns, British Standards Institution, London, UK.
[57] CNR-DT-201 (2005) 'Guideline for the design and construction of externally bonded FRP systems for strengthening existing structures - timber structures' Rome: Advisory Committee on Technical Recommendations for Construction.